

Doping dependence of antiferromagnetism in models of the pnictides

Jacob Schmiedt,* P. M. R. Brydon,† and Carsten Timm‡

Institut für Theoretische Physik, Technische Universität Dresden, 01062 Dresden, Germany

(Dated: February 24, 2012)

We study the doping dependence of the spin-density-wave (SDW) state in four models of the 1111 pnictides. The random-phase approximation is used to determine the ordering temperature and the ordering vector as functions of doping, and to evaluate the contribution of the various orbitals to the SDW instability. In addition to the usual assumption of orbitally rotation-invariant interactions, we consider the effect of reduced interactions involving the xy orbital, which are anticipated by crystal-structure considerations. We find that changing the relative strength of the interaction in the xy orbital tunes the system between different nesting instabilities leading to similar SDW order. We identify two models as showing reasonable agreement with experiments, while the other two display significant discrepancies, and discuss the underlying differences between the models.

PACS numbers: 74.50.+r, 74.20.Rp

I. INTRODUCTION

The discovery of superconductivity in the iron pnictides has triggered intense research activity striving to understand this diverse class of materials. Two pnictide families have attracted particular interest due to their high critical temperatures, namely the 1111 compounds¹ $R\text{FeAsO}$ and the 122 compounds² $A\text{Fe}_2\text{As}_2$ (R and A are rare-earth and alkaline-earth elements, respectively). Both systems are antiferromagnets at parent-compound filling, and must be chemically doped or subjected to significant pressure to become superconducting. The close proximity of antiferromagnetic (AFM) and superconducting states in the phase diagram evidences an intimate connection between the magnetic and the superconducting phases.^{3,4}

There is considerable experimental evidence that the 1111 and the 122 families display a metallic spin-density-wave (SDW) state.^{5–11} Furthermore, spectroscopic measurements indicate at most intermediate correlation strengths.^{12,13} This suggests that the microscopic origin of the AFM phase can be understood within a weak-coupling picture, which is consistent with *ab initio* calculations identifying the nesting between the electron and hole Fermi pockets as responsible for the SDW.^{14–16}

The nesting picture of the magnetism implies a strong doping dependence of the AFM phase. It is well established that the SDW critical temperature T_c of the 1111 compounds decreases upon electron doping.⁵ In contrast, very few experiments with hole-doped 1111 compounds have been reported, and the magnetic behavior remains obscure.^{17–21} The resistivity anomaly characteristic of the onset of SDW in the parent compounds becomes much less pronounced upon hole doping in $\text{La}_{1-x}\text{Sr}_x\text{FeAsO}$,^{17,18} $\text{Pr}_{1-x}\text{Sr}_x\text{FeAsO}$,¹⁹ and $\text{Pr}_{1-x}\text{Ca}_x\text{FeAsO}$,²⁰ but it is unclear whether this corresponds to a suppression of magnetic order. A more accurate probe of the antiferromagnetism is given by μSR measurements, which in $\text{Pr}_{1-x}\text{Sr}_x\text{FeAsO}$ suggests that mesoscopic phase separation allows a substantial fraction of the system to remain antiferromagnetic up to

$x = 0.2$, although it is not known if this is intrinsic.²¹ The experimental situation is much clearer in the 122 family, e.g., *electron-doping* rapidly suppresses the SDW in $\text{Ba}(\text{Fe}_{1-x}\text{Co}_x)_2\text{As}_2$, the SDW is already absent for $x = 0.05$,²² while for the *hole-doped* $\text{Ba}_{1-x}\text{K}_x\text{Fe}_2\text{As}_2$, and the SDW T_c decreases more slowly and vanishes at $0.3 < x < 0.4$, corresponding to 0.15–0.2 holes per single-Fe unit cell.^{23,24} It is interesting to see whether this asymmetric doping dependence of the AFM order can be replicated by theoretical models.

The complicated structure of the Fermi surface of the pnictides, which consists of two electron pockets and up to three hole pockets of various orbital character, allows for a number of different nesting instabilities that may compete with or reinforce each other. Previous works have identified two instabilities that may be responsible for the characteristic $(\pi, 0)$ order: Many authors^{25–34} identify the most important nesting as that between the hole pockets around the Γ point and the electron pocket at the X point of the single-Fe Brillouin zone, which implies a dominant role of the Fe $3d\ xz$ and yz orbitals in the formation of the SDW state. On the other hand, the role of nesting between the pockets at the Y and M points has also been emphasized,^{35–39} where the key contribution comes from the Fe $3d\ xy$ orbital. The two nesting instabilities are not mutually exclusive, and appear at similar doping levels. However, the number and location of the hole pockets involved in the magnetic instability nevertheless has important consequences for the spin wave spectrum^{28,40} and the realized commensurate SDW order.⁴¹ One of the goals of this work is therefore to examine the relative importance of the two nesting instabilities across the phase diagram.

The most popular starting point for the theoretical description of the pnictides are extended Hubbard models possessing orbital degrees of freedom. These models typically include up to five of the Fe $3d$ orbitals^{26,30,38,39,42–47} or also the As $4p$ orbitals.^{48,49} Since the former dominate the Fermi surface,^{14,50,51} models constructed in terms of the five Fe $3d$ orbitals are expected to give a good account of the physics while keeping the parame-

ter space manageable. In the study of these models it is common to assume orbitally rotation-invariant interactions.^{26,30,34–39,42–44,48,49,52,53} This symmetry is however broken by the underlying crystal structure of the FeAs lattice. Furthermore, upon integrating out the As 4*p* orbitals to obtain an effective Fe 3*d* model, the maximally localized Wannier functions of the 3*d* orbitals acquire a significant As 4*p* component, and are consequently expanded compared to the atomic limit.^{47,51} The *xy* orbital has the greatest overlap with the relevant 4*p* states and hence the greatest extent, which implies a weaker intraorbital interaction strength. Conversely, the $x^2 - y^2$ and $3z^2 - r^2$ orbitals have only small overlap with the 4*p* orbitals and are thus expected to remain rather compact, with stronger interaction potentials. The degenerate *xz* and *yz* orbitals lie in between these extremes. Miyake *et al.*⁴⁷ have confirmed the expected hierarchy of interaction strengths within a constrained random-phase approximation (cRPA). The *xz*, *yz*, and *xy* orbitals make up the bulk of the Fermi surface,⁵⁰ and so they are most important when considering the origin of the SDW. The relatively weaker interaction strength on the *xy* orbital might therefore be expected to play a significant role in selecting the leading nesting instability. Investigating this aspect of the physics is the second major goal of our paper.

In order to answer these questions we consider the doping dependence of the magnetic order in four different five-orbital models of LaFeAsO, proposed by Kuroki *et al.*,⁴² Graser *et al.*,⁴³ Ikeda *et al.*,³⁹ and Calderón *et al.*⁴⁶ All four models are based on *ab initio* band structures. Kuroki *et al.* and Ikeda *et al.* obtain tight-binding models from LDA calculations employing maximally localized Wannier functions, while Graser *et al.* fit a Slater-Koster tight-binding model to a GGA band structure. Calderón *et al.* propose a Slater-Koster model containing a limited number of free parameters, which were chosen to best reproduce the LDA band structure. We employ the random-phase approximation (RPA) to calculate the static spin susceptibility in the paramagnetic phase, and examine it for divergences as the temperature and doping are varied. This allows us to determine the limits of the paramagnetic state in an unbiased way as we are able to identify ordered states with large unit cells that would not be accessible by the usual mean-field approaches.^{26,30,34,44,52,53} Further insight into the nesting mechanisms in the models is obtained by decomposing the paramagnetic RPA spin susceptibility into its orbital components close to the critical temperature. The comparison of the magnetic phase diagrams of these models is the final major goal of our work. Not only does this allow us to better understand the mechanisms for antiferromagnetism in the pnictides, but also it helps to identify the most realistic models for this system.

The paper is organized as follows. In Sec. II we introduce the model Hamiltonian and outline the calculation of the RPA spin susceptibility. We proceed to conduct a systematic analysis of the four different models in Sec. III. This is followed in Sec. IV by a discussion of our re-

sults and the implications for the understanding of the pnictides. We conclude with a summary in Sec. V.

II. THEORY

A. Model

We start with a tight binding Hamiltonian that describes the non-interacting five-orbital system

$$H_0 = \sum_{\mathbf{k}} \sum_{\sigma} \sum_{\nu, \mu} T_{\nu, \mu}(\mathbf{k}) d_{\mathbf{k}, \nu, \sigma}^{\dagger} d_{\mathbf{k}, \mu, \sigma}, \quad (1)$$

where $d_{\mathbf{k}, \nu, \sigma}^{\dagger}$ ($d_{\mathbf{k}, \nu, \sigma}$) is the creation (annihilation) operator for a spin σ electron of momentum \mathbf{k} in the orbital ν . The values of $T_{\nu, \mu}$ for the different models are provided in Refs. 42, 43, 39, and 46. Keeping only local terms in the interaction Hamiltonian, we have

$$\begin{aligned} H_{\text{int}} = & \sum_{\mathbf{i}} \sum_{\nu \mu} \sum_{\sigma \sigma'} \left[U_{\nu \mu} d_{\mathbf{i}, \nu, \sigma}^{\dagger} d_{\mathbf{i}, \mu, \sigma'}^{\dagger} d_{\mathbf{i}, \mu, \sigma'} d_{\mathbf{i}, \nu, \sigma} \right. \\ & + J_{\nu \mu} \left(d_{\mathbf{i}, \nu, \sigma}^{\dagger} d_{\mathbf{i}, \mu, \sigma'}^{\dagger} d_{\mathbf{i}, \nu, \sigma'} d_{\mathbf{i}, \mu, \sigma} \right. \\ & \left. \left. + d_{\mathbf{i}, \nu, \sigma}^{\dagger} d_{\mathbf{i}, \nu, \sigma'}^{\dagger} d_{\mathbf{i}, \mu, \sigma} d_{\mathbf{i}, \mu, \sigma'} \right) \right], \quad (2) \end{aligned}$$

where the index \mathbf{i} stands for the lattice site, ν and μ stand for the orbitals, and σ and σ' denote the spin. Equation (2) is usually^{26,30,34–39,42–44,48,52,53} simplified by assuming orbital-independent interactions for which we then have

$$\begin{aligned} H_{\text{int}} = & U \sum_{\mathbf{i}} \sum_{\nu} n_{\mathbf{i}, \nu, \uparrow} n_{\mathbf{i}, \nu, \downarrow} \\ & + \frac{1}{4} (2U - 5J) \sum_{\mathbf{i}} \sum_{\nu \neq \mu} \sum_{\sigma, \sigma'} n_{\mathbf{i}, \nu, \sigma} n_{\mathbf{i}, \mu, \sigma'} \\ & - J \sum_{\mathbf{i}} \sum_{\nu \neq \mu} \mathbf{S}_{\mathbf{i}, \nu} \cdot \mathbf{S}_{\mathbf{i}, \mu} \\ & + J \sum_{\mathbf{i}} \sum_{\nu \neq \mu} d_{\mathbf{i}, \nu, \uparrow}^{\dagger} d_{\mathbf{i}, \nu, \downarrow}^{\dagger} d_{\mathbf{i}, \mu, \downarrow} d_{\mathbf{i}, \mu, \uparrow}. \quad (3) \end{aligned}$$

This is obtained from Eq. (2) by setting $U_{\nu \nu} = U$, $J_{\nu \mu} = J$ and $U_{\nu \mu} = \frac{1}{4}(2U - 5J)$ if $\nu \neq \mu$. The latter choice implies invariance of the interaction Hamiltonian under rotations in orbital space.^{54,55} The spin operators are expressed in terms of the creation and annihilation operators as $\mathbf{S}_{\mathbf{i}, \nu} = \frac{1}{2} \sum_{\sigma \sigma'} d_{\mathbf{i}, \nu, \sigma}^{\dagger} \boldsymbol{\sigma}_{\sigma \sigma'} d_{\mathbf{i}, \nu, \sigma'}$, where $\boldsymbol{\sigma}$ is the vector of Pauli matrices. The ratio between the local Coulomb interaction and the Hund's rule coupling is set to $U/J = 4$. For our calculations we adopt the standard assumption that doping does not change the interaction and band structure parameters in the Hamiltonian.

Although the invariance of the interaction Hamiltonian under orbital rotations is a common assumption,^{26,30,34–39,42–44,48,49,52,53} in general we expect different interaction strengths $U_{\nu, \nu}$ and $J_{\nu, \nu}$ for inequivalent

choices of the orbitals μ, ν . In particular, of the three orbitals which dominate the electronic structure near the Fermi surface, *ab initio* calculations of Miyake *et al.*⁴⁷ predict a much weaker interaction on the xy orbital compared to the equivalent xz and yz orbitals. In order to capture this aspect of the physics we renormalize every interaction strength in Eq. (3) involving the xy orbital by a multiplicative factor of $V_{xy} \leq 1$; all other interactions are left unchanged.

B. Method

The static paramagnetic spin susceptibility contains all necessary information about the magnetic instabilities of the paramagnetic state. In particular, it diverges at the ordering vector as one approaches the critical temperature T_c . Hence, a temperature-vs.-doping phase diagram for the boundaries of the paramagnetic phase can be obtained by determining the highest temperature for which $1/\chi_s(\mathbf{q}, 0)$ vanishes as the filling is varied, where the corresponding \mathbf{q} is the ordering vector \mathbf{Q} . We obtain the static susceptibility from the analytic continuation $i\omega_n \rightarrow \omega + i0^+$ of the total susceptibility in Matsubara-frequency space and subsequently taking the limit $\omega \rightarrow 0$. The total spin susceptibility is defined as

$$\begin{aligned} \chi_s(\mathbf{q}, i\omega_n) &= \frac{1}{N} \sum_{j,j'=x,y,z} \sum_{\nu\mu} \int_0^\beta d\tau e^{i\omega_n\tau} \langle T_\tau S_\nu^j(\mathbf{q}, \tau) S_\mu^{j'}(-\mathbf{q}, 0) \rangle. \end{aligned} \quad (4)$$

The Fourier-transformed spin operator $S_\nu^j(\mathbf{q})$ is related to the spin operator at site \mathbf{i} by

$$S_{\mathbf{i},\nu}^j = \frac{1}{\sqrt{N}} \sum_{\mathbf{q}} S_\nu^j(\mathbf{q}) e^{-i\mathbf{q}\cdot\mathbf{r}_\mathbf{i}}.$$

Due to rotational symmetry in the paramagnetic phase, the spin susceptibility can be expressed in terms of its transverse part

$$\chi_s(\mathbf{q}, 0) = \frac{3}{2} \chi^{-+}(\mathbf{q}, 0). \quad (5)$$

The transverse susceptibility is written as

$$\chi^{-+}(\mathbf{q}, i\omega_n) = \sum_{\nu,\mu} \chi_{\nu\nu\mu\mu}^{-+}, \quad (6)$$

where we introduce the generalized susceptibility

$$\begin{aligned} \chi_{\nu\nu'\mu\mu'}^{-+}(\mathbf{q}, i\omega_n) &= \frac{1}{N} \sum_{\mathbf{k}, \mathbf{k}'} \int_0^\beta d\tau e^{i\omega_n\tau} \\ &\times \langle T_\tau d_{\mathbf{k}+\mathbf{q},\nu,\downarrow}^\dagger(\tau) d_{\mathbf{k},\nu',\uparrow}(\tau) d_{\mathbf{k}'-\mathbf{q},\mu,\uparrow}^\dagger(0) d_{\mathbf{k}',\mu',\downarrow}(0) \rangle. \end{aligned} \quad (7)$$

The orbitally resolved susceptibilities $\chi_{\nu\nu\mu\mu}^{-+} \equiv \chi_{\nu\mu}^{-+}$ are of particular interest, as they contain information about the contribution of the different orbitals to the instability.

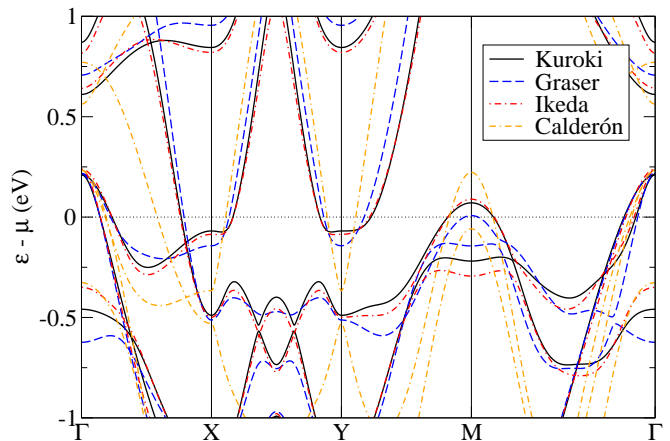


FIG. 1. (color online) Band structure along high-symmetry lines for the four models of Refs. 39, 42, 43, and 46.

We calculate $\chi_{\nu\mu}^{-+}$ using the RPA. Summing up the ladder diagrams, we obtain the Dyson equation

$$\chi_{\nu\nu\mu\mu}^{-+} = \chi_{\nu\nu\mu\mu}^{-+(0)} + \chi_{\nu\nu\alpha\beta}^{-+(0)} V_{\alpha\beta\gamma\delta} \chi_{\gamma\delta\mu\mu}^{-+}, \quad (8)$$

where the non-zero elements of $V_{\alpha\beta\gamma\delta}$ are given by

$$V_{aaaa} = U[1 - (1 - V_{xy})\delta_{a,xy}] \quad (9a)$$

$$V_{aabb} = J[1 - (1 - V_{xy})(\delta_{a,xy} + \delta_{b,xy})] \quad (9b)$$

$$V_{abba} = (U - 2J)[1 - (1 - V_{xy})(\delta_{a,xy} + \delta_{b,xy})] \quad (9c)$$

$$V_{abab} = J[1 - (1 - V_{xy})(\delta_{a,xy} + \delta_{b,xy})] \quad (9d)$$

with $a \neq b$. The bare susceptibilities $\chi_{\nu\nu'\mu\mu'}^{-+(0)}$ are given by

$$\begin{aligned} \chi_{\nu\nu'\mu\mu'}^{-+(0)}(\mathbf{q}, i\omega_n) &= -\frac{1}{N} \sum_{\mathbf{k}} \sum_{s,s'} u_{s,\nu'}(\mathbf{k}) u_{s,\mu}^*(\mathbf{k}) u_{s',\mu'}(\mathbf{k} + \mathbf{q}) u_{s',\nu}^*(\mathbf{k} + \mathbf{q}) \\ &\times \frac{n_F(E_{s,\mathbf{k}}) - n_F(E_{s',\mathbf{k}+\mathbf{q}})}{E_{s,\mathbf{k}} - E_{s',\mathbf{k}+\mathbf{q}} - i\omega_n}, \end{aligned} \quad (10)$$

where $n_F(E)$ is the Fermi function, $E_{\mathbf{k}}$ are the eigenvalues of H_0 , and $u_{s,\nu}(\mathbf{k})$ are the coefficients that transform the annihilation operators of the diagonalizing basis $\gamma_{s,\mathbf{k}}$ into the orbital basis, i.e., $d_{\nu,\mathbf{k}} = \sum_s u_{s,\nu}(\mathbf{k}) \gamma_{s,\mathbf{k}}$. We adopt the common approximation to ignore Hartree shifts,^{36,43,44,52} as we assume them to be included in the *ab initio* calculations. We have verified that the inclusion of Hartree shifts only leads to small quantitative changes in our results.

III. RESULTS

In this section we present our analysis of the four different five-orbital models.^{39,42,43,46} We first investigate the temperature-vs.-doping phase diagrams, calculated as described in section II B. The summation over \mathbf{k} in

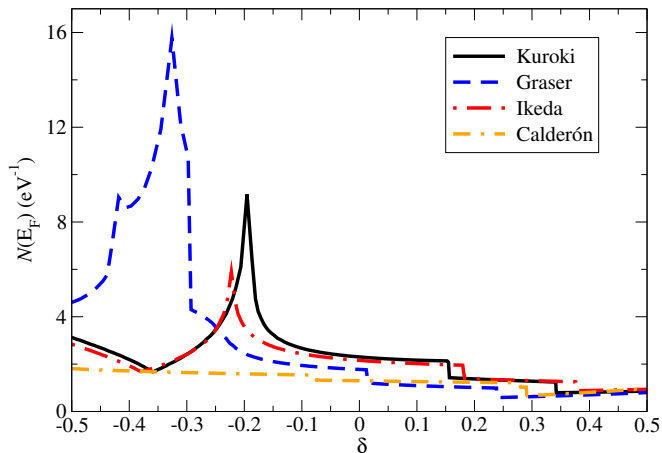


FIG. 2. (color online) Density of states at the Fermi level as a function of the doping δ , related by the electron concentration by $n = 6 + \delta$, for the four band structures from Fig. 1.

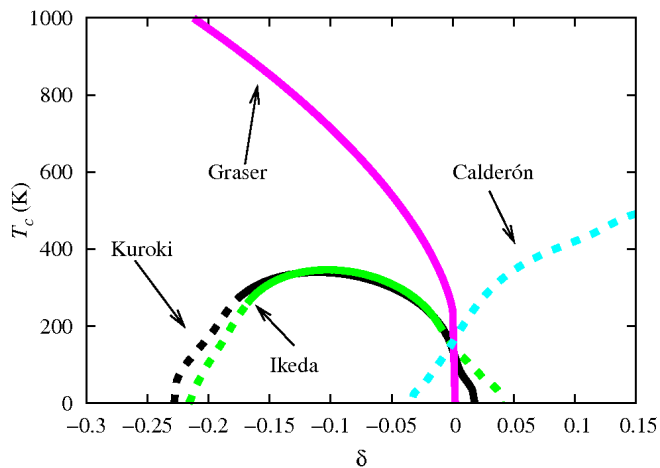


FIG. 3. (color online) Critical temperature as a function of doping δ for the four models from Fig. 1 with $V_{xy} = 1$, see text. Solid lines denote $(\pi, 0)$ order, whereas dashed lines denote incommensurate order. The interaction strengths were chosen as $U = 0.875$ eV for Kuroki *et al.*,⁴² $U = 0.885$ eV for Ikeda *et al.*,³⁹ $U = 1.2232$ eV for Graser *et al.*,⁴³ and $U = 1.383$ eV for Calderón *et al.*⁴⁶

Eq. (10) was performed using a 400×400 \mathbf{k} -point mesh. We have checked that a 200×200 \mathbf{k} -point mesh results in only small quantitative differences and so finite size effects are expected to be negligible. We ignore ordered states with critical temperatures less than 10K. Throughout we measure the doping δ relative to parent compound filling, i.e., the electron concentration is $n = 6 + \delta$.

We start by discussing the non-interacting system. In Fig. 1 we plot the non-interacting band structure of the undoped models close to the Fermi energy. The models of Kuroki *et al.*⁴² and Ikeda *et al.*³⁹ are hardly distinguishable within about 0.1 eV of the Fermi surface, and

so we expect a very similar phase diagram for these two models at weak doping. Near to the Γ point, the Fermi surfaces for the model of Graser *et al.*⁴³ almost coincide with those of Kuroki *et al.* and Ikeda *et al.*, but elsewhere there are significant differences: The hole pocket at the M point is very small compared to these models, the electron pocket at the X point is also smaller, and the $(3z^2 - r^2)$ -derived flat band at the M point lies much closer to the Fermi energy. The model of Calderón *et al.*⁴⁶ is quite distinct from the other models, with highly elliptical electron pockets, almost degenerate hole pockets at the Γ point, and no flattening of the $(3z^2 - r^2)$ -derived band at the M point.

The density of states as a function of doping, shown in Fig. 2, provides additional insight. The models of Ikeda *et al.*³⁹ and Kuroki *et al.*⁴² both show a peak in the density of states close to $\delta = -0.2$, although it is significantly larger in the latter. This peak arises from the flat bottom of the electron band at the X point. The model of Graser *et al.*⁴³ also shows a very high density of states below $\delta = -0.3$ that is connected to the $(3z^2 - r^2)$ -derived flat band at the M point. These peaks raise the possibility of a competition between AFM and ferromagnetic order at strong hole doping.⁵⁶ In contrast, the model of Calderón *et al.*⁴⁶ has an almost featureless density of states, due to the much lower bottom of the electron bands and the absence of the $(3z^2 - r^2)$ -derived flat band at the M point.

In order to study the doping dependence of the AFM phase we first choose the interaction strength U for each model such that at $\delta = 0$ the critical temperature is $T_c \approx 150$ K, close to the experimentally observed ordering temperature. The resulting temperature-vs.-doping phase diagrams for all four models are shown in Fig. 3. All models show an enhancement of T_c for non-zero doping. The dome structure of T_c with a maximum at moderate hole doping ($\delta \approx -0.1$) for the models of Kuroki *et al.*⁴² and Ikeda *et al.*³⁹ is consistent the phase diagram determined by Ikeda *et al.* in Ref. 39. In contrast, the monotonous increase of T_c in the model of Graser *et al.*⁴³ for strong hole doping, and the enhancement of magnetic order for *electron* doping in the model of Calderón *et al.*,⁴⁶ are contradicted by experiments. The model of Calderón *et al.* further deviates from experimental findings by displaying a highly incommensurate ordering vector $\mathbf{Q} = (\pi, 0.24\pi)$ at zero doping.

The models of Kuroki *et al.* and Ikeda *et al.* are most consistent with the reported asymmetric doping-dependence of the AFM in the pnictides, although the optimal critical temperature is much too high. Note that there is no reason to assume that the undoped *three-dimensional* parent compounds are best described by choosing precisely the value $\delta = 0$ in these *two-dimensional* models. Moreover, we will see that a moderate increase of the onsite energy of the xy orbital shifts the peak position to $\delta = 0$ for some of the models. Instead of specifying T_c at $\delta = 0$ as in Fig. 3, it is therefore more reasonable to search for an interaction strength giving a dome shape of T_c and an ordering temperature of

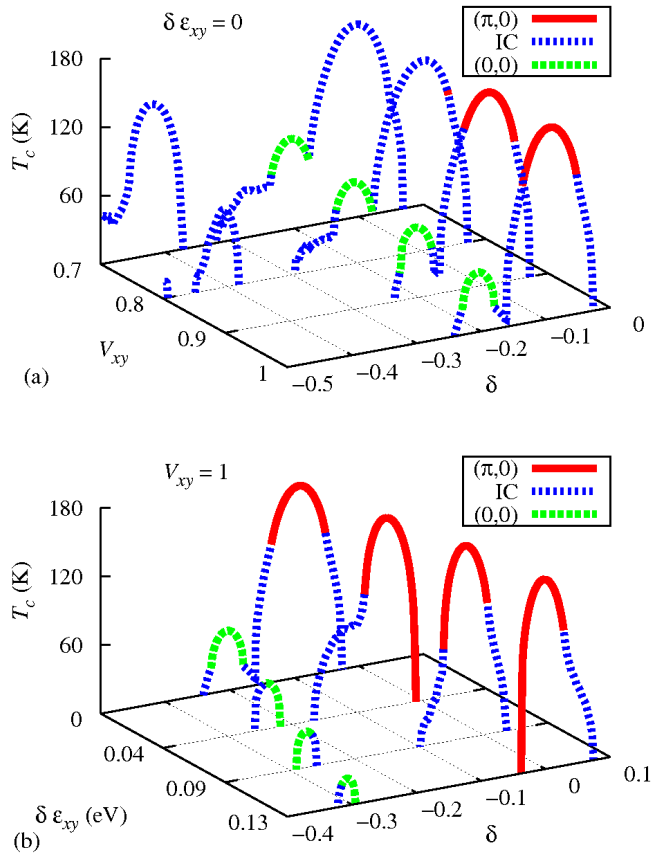


FIG. 4. (color online) (a) Doping dependence of the critical temperature for the model of Kuroki *et al.*⁴² at different values of V_{xy} . To maintain $T_c^{\text{opt}} \approx 165$ K, we choose $U = 0.8$ eV for $V_{xy} = 1$, $U = 0.845$ eV for $V_{xy} = 0.9$, $U = 0.885$ eV for $V_{xy} = 0.8$, and $U = 0.915$ eV for $V_{xy} = 0.7$. (b) Doping dependence of the critical temperature for different shifts of the xy -orbital on-site energy $\delta\varepsilon_{xy}$ with respect to the value given in Ref. 42. For constant optimal doping critical temperature $T_c^{\text{opt}} \approx 165$ K we choose $U = 0.8$ eV for $\delta\varepsilon_{xy} = 0$ eV, $U = 0.782$ eV for $\delta\varepsilon_{xy} = 1.04$ eV, $U = 0.78$ eV for $\delta\varepsilon_{xy} = 1.09$ eV, and $U = 0.785$ eV for $\delta\varepsilon_{xy} = 1.13$ eV.

$T_c^{\text{opt}} \approx 165$ K at a non-zero optimal doping δ . The lower T_c^{opt} should also allow us to unambiguously identify the leading nesting instabilities responsible for the SDW. Below we construct the phase diagram of each model according to this argument.

A. The model of Kuroki *et al.*

The phase diagram for the model of Kuroki *et al.*⁴² is shown in Fig. 4. Initially focusing on the case of $V_{xy} = 1$, we still find a dome of $(\pi, 0)$ order centered at the optimal doping $\delta = -0.093$, but there is no magnetic order at $\delta = 0$. In addition to the AFM dome, there is also a region of ferromagnetic order around $\delta = -0.2$. The highest critical temperature of the ferromagnetic state

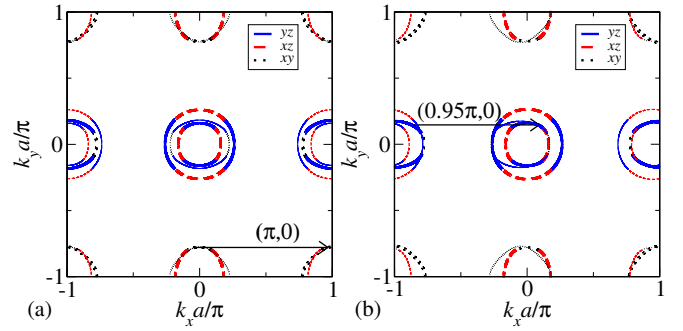


FIG. 5. (color online) Fermi surface for the model of Kuroki *et al.*⁴² (heavy lines) superimposed with the Fermi surface shifted by (a) $(\pi, 0)$ for $\delta = -0.093$ and (b) $(0.95\pi, 0)$ for $\delta = -0.105$ (thin lines), corresponding to the ordering at optimal doping for $V_{xy} = 1$ and $V_{xy} = 0.7$, respectively.

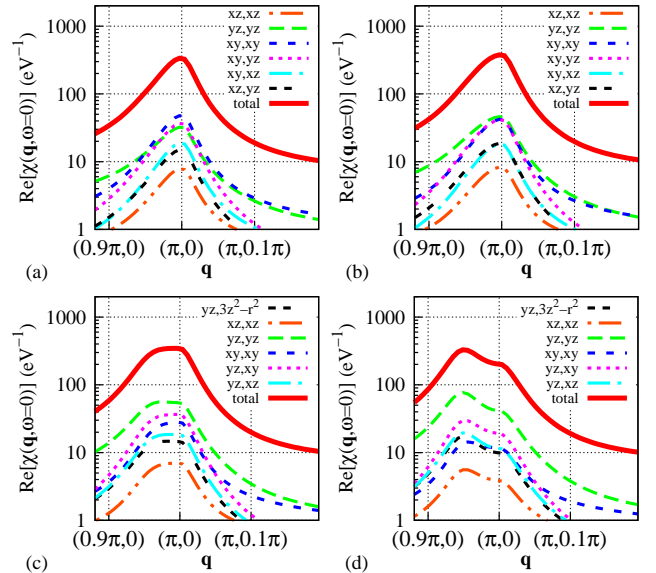


FIG. 6. (color online) Total susceptibilities and orbitally resolved contributions $\chi_{\nu\mu}^{-+}$ at $T = 180$ K for the model of Kuroki *et al.*⁴² at (a) $V_{xy} = 1$, $\delta = -0.093$, (b) $V_{xy} = 0.9$, $\delta = -0.092$, (c) $V_{xy} = 0.8$, $\delta = -0.096$, and (d) $V_{xy} = 0.7$, $\delta = -0.105$.

occurs close to the peak in the density of states, see Fig. 2, consistent with the Stoner criterion.

The mechanism responsible for the $(\pi, 0)$ order can be observed most clearly at the optimal doping $\delta = -0.093$. As shown in Fig. 5(a), here we find excellent nesting of the xy -orbital-dominated parts of the electron pocket at the Y point with the xy -derived hole pocket at the M point, suggesting that these Fermi surfaces play the leading role in the AFM instability. A further hint that the xy orbital is most important for the AFM order comes from the observation that the optimal doping can be shifted to $\delta = 0$ by increasing the on-site energy of the xy orbital

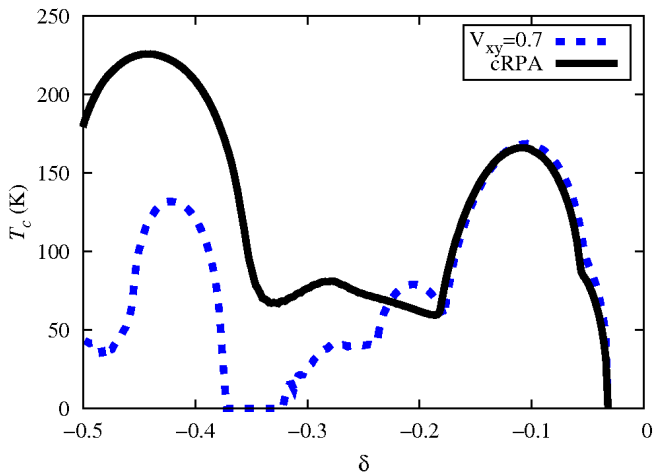


FIG. 7. (color online) Doping dependence of the critical temperature for the model of Kuroki *et al.*⁴² for $V_{xy} = 0.7$ (dashed) and for the fully orbital-dependent interactions predicted in Ref. 47 (solid). For the latter, the interactions strengths were scaled by 0.406 to find a maximal ordering temperature of $T_c \approx 165$ K at $\delta > -0.2$. Both calculations yield an ordering vector $\mathbf{Q} = (0.95\pi, 0)$ at the maximum T_c close to $\delta = -0.1$.

by ~ 0.1 eV [see Fig. 4(b)], and always coincides with good nesting of the Y and M pockets.

To examine the effect of the likely weaker interactions in the xy orbital, in Fig. 4(a) we plot the evolution of the phase diagram upon reducing V_{xy} while simultaneously increasing U such that T_c^{opt} remains constant. At $V_{xy} = 0.7$, which is close to the value predicted by Miyake *et al.*,⁴⁷ we find that the optimal doping of the AFM dome shifts to $\delta = -0.105$, and the ordering vector at this filling becomes weakly incommensurate with $\mathbf{Q} = (0.95\pi, 0)$. The Fermi surface plotted in Fig. 5(b) shows that this corresponds to good nesting between the hole pockets at the Γ point and the electron pocket at the X point, where the best-nested segments of the Fermi surface have mostly yz -orbital character. The necessary increase of U by $\sim 10\%$ when V_{xy} is reduced implies that the AFM instability due to Γ -X nesting requires a significantly higher interaction than the Y-M nesting to produce a realistic T_c^{opt} . Additional magnetically ordered states appear at strong doping $\delta \approx -0.42$ with optimal ordering vector $\mathbf{Q} = (0.44\pi, 0)$. At these doping levels, however, our assumption of rigid bands is questionable and so the physical relevance of these results is doubtful.

Greater insight into the origin of the AFM order can be achieved by examining the orbitally resolved susceptibilities at optimal doping just above T_c , see Fig. 6. As V_{xy} is decreased, the dominant contribution shifts from the susceptibilities $\chi_{\nu\mu}^{-+}$ involving the xy orbital to those involving the yz orbital, and the peak in $\chi_{\nu\mu}^{-+}$ moves from $(\pi, 0)$ to an incommensurate vector. This is in perfect agreement with the observed change of the nesting from xy -dominated to yz -dominated parts of the Fermi sur-

face. By changing V_{xy} we can therefore select the dominant nesting instability of the system.

Our treatment of the weaker interaction on the xy orbital neglects the likely different interaction strengths involving the other inequivalent orbitals. To test our approximation, we compare the $V_{xy} = 0.7$ phase diagram of Fig. 4(a) with the phase diagram calculated using Miyake *et al.*'s⁴⁷ cRPA values for $U_{\nu\mu}$ and $J_{\nu\mu}$ in Eq. (2). As shown in Fig. 7, upon suitably rescaling the cRPA interaction potentials, we find excellent agreement between the two phase diagrams for the physically reasonable doping regime $\delta > -0.2$. We note that in the fully orbital-dependent results we have to choose a slightly larger value of $U_{yz,yz}$ than in our $V_{xy} = 0.7$ calculations in order to achieve $T_c^{\text{opt}} \approx 165$ K for the peak around $\delta \approx -0.1$; the origin of this discrepancy is likely the weaker exchange interaction $J_{\nu\mu} < 0.25 U_{\nu\nu}$ predicted by Ref. 47. This also indicates that the AFM order does not crucially depend upon the ratio U/J in the weak-coupling regime. For strong doping, larger deviations appear, in particular there is no ferromagnetism for the cRPA interactions, and the critical temperature of the incommensurate AFM state at $\delta \approx -0.4$ is higher although the ordering vector is similar.

B. The model of Graser *et al.*

The phase diagram for the model of Graser *et al.*⁴³ is shown in Fig. 8(a). At $V_{xy} = 1$ we find a dome of commensurate AFM order centered at $\delta = -0.12$ and also a small incommensurate dome with $\mathbf{Q} = (0.95\pi, 0)$ at $\delta \approx -0.05$. At $\delta < -0.2$ we observe an incommensurate AFM state with ordering vector $\mathbf{Q} = (0.71\pi, 0)$, and a high critical temperature, which strongly increases with hole doping. The strong tendency to AFM order at strong hole doping occurs only in this model, and is likely connected with the $(3z^2 - r^2)$ -derived flat band at the M point. Indeed, a Fermi surface due to this band appears at the critical doping level for the incommensurate AFM order. Furthermore, the ordering at strong doping can be suppressed by increasing the on-site energy of the xy orbital, which effectively lowers the flat band at the M point. This also shifts the optimal doping of the $(\pi, 0)$ dome at $\delta = -0.12$ towards zero, again suggesting an important role for the xy orbital in the $(\pi, 0)$ order.

Focusing our attention on the regime of moderate doping, $-0.2 < \delta < 0$, we find that as V_{xy} is reduced, the small incommensurate dome grows and becomes the leading instability at $V_{xy} = 0.7$. At this value of V_{xy} , the ordering vector at optimal doping $\delta = -0.06$ is $\mathbf{Q} = (0.93\pi, 0)$. The orbitally resolved susceptibilities at the optimal doping of the $(\pi, 0)$ order at $V_{xy} = 1$ and the incommensurate order for $V_{xy} = 0.7$ are plotted in Figs. 8(b) and (c), respectively, while the nesting of the corresponding Fermi surfaces are shown in Figs. 8(d) and (e). These results are very similar to those obtained for the model of Kuroki *et al.*,⁴² see Figs. 6 and 5. We hence

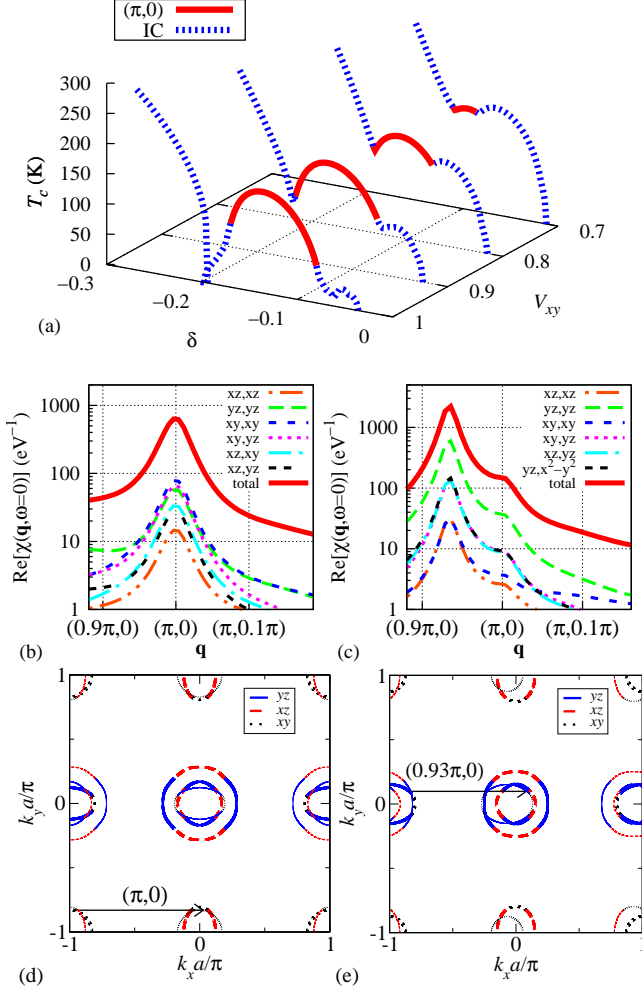


FIG. 8. (color online) (a) Doping dependence of the critical temperature for the model of Graser *et al.*⁴³ at different values of V_{xy} . To maintain $T_c^{\text{opt}} \approx 165$ K, we choose $U = 1.09$ eV for $V_{xy} = 1$, $U = 1.146$ eV for $V_{xy} = 0.9$, $U = 1.191$ eV for $V_{xy} = 0.8$, and $U = 1.222$ eV for $V_{xy} = 0.7$. (b) The total susceptibility and the largest $\chi_{\nu\mu}^-$ for $V_{xy} = 1$, $T = 180$ K, and the optimal doping $\delta = -0.137$ of the $(\pi, 0)$ state. (c) Same as in (b) but for $V_{xy} = 0.7$, $T = 180$ K, and the optimal doping $\delta = -0.065$ of the incommensurate state. (d) Fermi surface at $\delta = -0.137$ (heavy lines) with the same Fermi surface shifted by $(\pi, 0)$ superimposed (thin lines). (e) Fermi surface at $\delta = -0.065$ (heavy lines) with the same Fermi surface shifted by $(0.93\pi, 0)$ superimposed (thin lines).

conclude that again a reduction of V_{xy} tunes the system from the xy -dominated to the yz -dominated instability, although the optimal dopings for the two instabilities are more widely separated than in the model of Kuroki *et al.* This can be explained by the small M pocket at zero doping in Graser *et al.*'s model,⁴³ which implies a much larger change of the doping in order to optimize the Y-M nesting. Furthermore, due to the smaller size of the electron

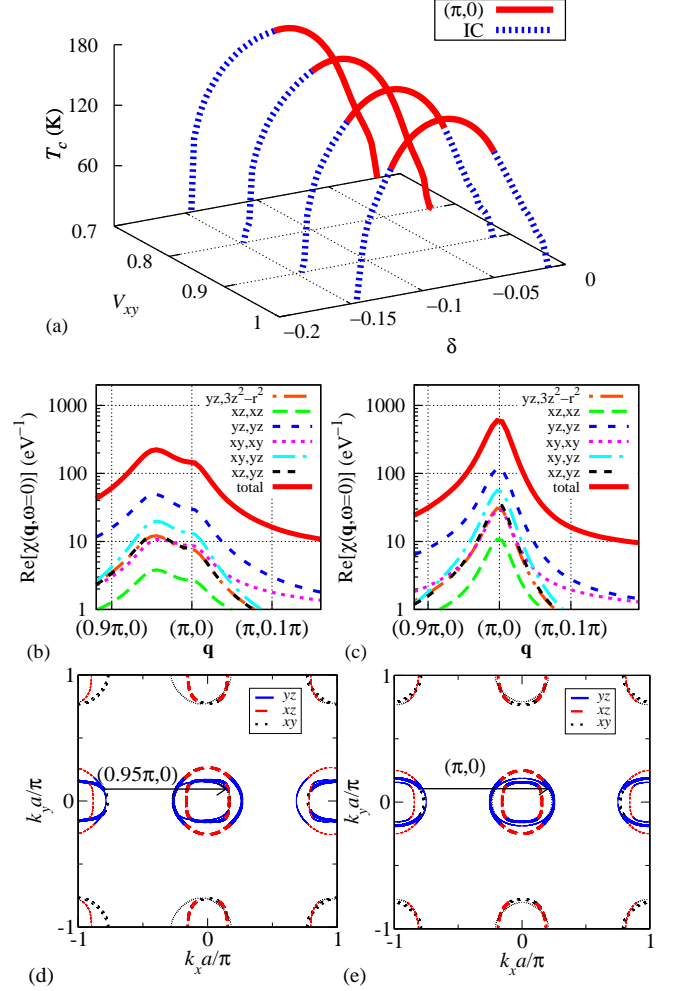


FIG. 9. (color online) (a) Doping dependence of the critical temperature for the model of Ikeda *et al.*³⁹ at different values of V_{xy} . To maintain $T_c^{\text{opt}} \approx 165$ K, we choose $U = 0.808$ eV for $V_{xy} = 1$, $U = 0.852$ eV for $V_{xy} = 0.9$, $U = 0.892$ eV for $V_{xy} = 0.8$, and $U = 0.925$ eV for $V_{xy} = 0.7$. (b) The total susceptibility and the largest $\chi_{\nu\mu}^-$ for $V_{xy} = 0.7$, $T = 160$ K, and $\delta = -0.12$. (c) Same as in (b) but at $\delta = -0.06$. (d) Fermi surface at $\delta = -0.12$ (heavy lines) with the same Fermi surface shifted by $(0.95\pi, 0)$ superimposed (thin lines). (e) Fermi surface at $\delta = -0.06$ (heavy lines) with the same Fermi surface shifted by $(\pi, 0)$ superimposed (thin lines).

pockets at parent compound filling, the incommensurate AFM phase is stabilized at weaker doping.

C. The model of Ikeda *et al.*

The phase diagram for the model of Ikeda *et al.*³⁹ at $V_{xy} = 1$ [Fig. 9(a)] is very similar to that for the model of Kuroki *et al.*,⁴² although ferromagnetism is not found near $\delta = -0.2$, consistent with the smaller peak in the

density of states [Fig. 2]. The $(\pi, 0)$ order is again dominated by the xy orbital, and the nesting of the Y and M pockets is primarily responsible for the AFM state, in agreement with Ref. 39. Despite the very similar band structure to the model of Kuroki *et al.*, the phase diagram for $V_{xy} < 1$ shows a significant difference: The $(\pi, 0)$ order does not vanish for $V_{xy} = 0.7$, but instead moves to the low-doping half of the AFM dome while the other half is incommensurate. As for Kuroki *et al.*'s model, however, the yz orbital dominates the magnetism over the full doping range. This can be seen in two representative plots of $\chi_{\nu\mu}^{-+}$ in Figs. 9(b) and (c) at $\delta = -0.12$ and $\delta = -0.06$ which correspond to incommensurate $\mathbf{Q} = (0.95\pi, 0)$ and commensurate $\mathbf{Q} = (\pi, 0)$ ordering vectors, respectively. As revealed by Figs. 9(d) and (e), at both of these doping levels there is excellent nesting of the X and Γ pockets. The ordering vector tracks the continuous evolution of this nesting vector across the dome, from slightly incommensurate to commensurate. The close similarity of this model to the one of Kuroki *et al.* shows that very small differences in the band structure play a major role in determining the ordering vector.

D. The model of Calderón *et al.*

The phase diagram for the model of Calderón *et al.*,⁴⁶ shown in Fig. 10(a), is in stark contrast to those for the other models. The magnetic order is optimized at strong electron doping, $\delta \approx 0.18$, and occurs at the highly incommensurate ordering vector $\mathbf{Q} = (\pi, 0.39\pi)$. Although this is inconsistent with experimental findings for the pnictide systems, it is nevertheless interesting to examine the origin of this AFM state. An important clue comes from observing that the phase diagram hardly changes when V_{xy} is decreased, although the interaction U has to be increased in order to keep T_c^{opt} constant. This indicates that the xy orbital is almost exclusively responsible for the magnetic ordering, which is confirmed by the orbitally resolved susceptibilities presented in Figs. 10(b) and (c). The incommensurate ordering vector at optimal doping gives excellent nesting of the xy pocket at the M point and the xy -dominated tip of the electron Fermi surface at the Y point [Fig. 10(d)], revealing an unexpected similarity to the nesting instabilities in the other models.

The stabilization of AFM order by electron-doping in the model of Calderón *et al.* follows from the observation that the magnetic order arises only from Y-M nesting. In Fig. 1 it can be seen that at $\delta = 0$ the circular hole pocket at the M point has almost the same radius as in the models of Kuroki *et al.*⁴² and Ikeda *et al.*³⁹ In contrast, the ellipticity of the electron pockets is highly exaggerated in the model of Calderón *et al.*, and indeed the minor axis of the electron pockets is much smaller than the diameter of the M-point hole pocket. As such, it is necessary to raise the chemical potential (i.e., dope with electrons) to optimize the nesting between these two Fermi surfaces.

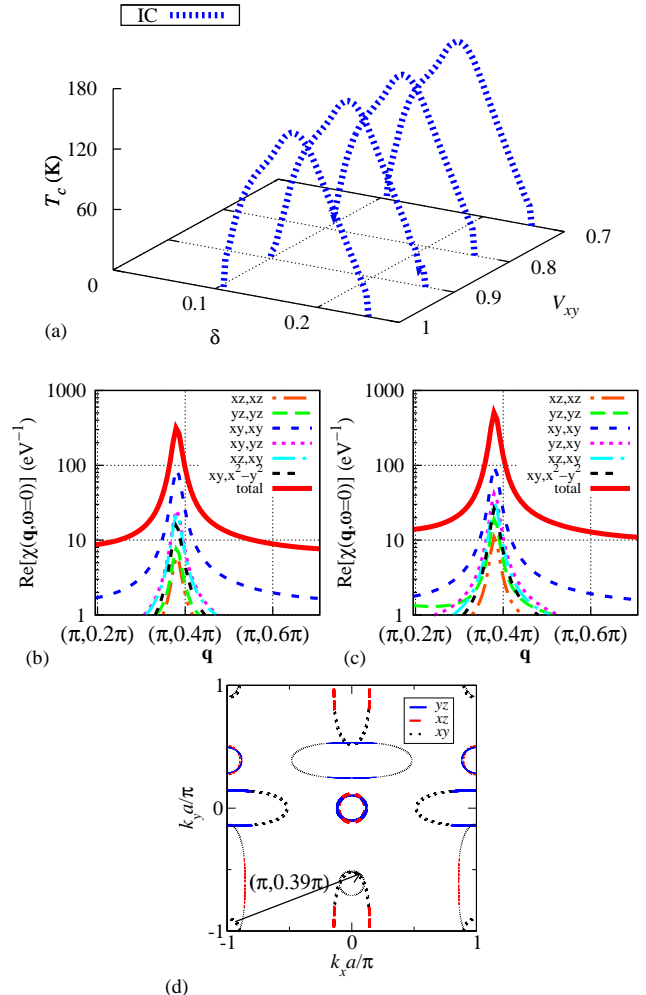


FIG. 10. (color online) (a) Doping dependence of the critical temperature for the model of Calderón *et al.*⁴⁶ at different values of V_{xy} . To maintain $T_c^{\text{opt}} \approx 165$ K, we choose $U = 1.269$ eV for $V_{xy} = 1$, $U = 1.378$ eV for $V_{xy} = 0.9$, $U = 1.498$ eV for $V_{xy} = 0.8$ and $U = 1.635$ eV for $V_{xy} = 0.7$. (b) The total susceptibility and the largest $\chi_{\nu\mu}^{-+}$ for $V_{xy} = 1$, $T = 180$ K, and $\delta = 0.176$. (c) Same as in (b) but for $V_{xy} = 0.7$. (d) Fermi surface at $\delta = 0.176$ (heavy lines) with the same Fermi surface shifted by $(\pi, 0.39\pi)$ superimposed (thin lines).

IV. DISCUSSION

Our study of the four different models for the 1111 pnictides shows a clear distinction between the models of Kuroki *et al.*,⁴² Graser *et al.*,⁴³ and Ikeda *et al.*³⁹ on the one hand and the model of Calderón *et al.*⁴⁶ on the other. In the former, a SDW is stabilized for hole doping with commensurate or near-commensurate ordering vector, whereas in the latter we find a strongly incommensurate AFM state upon electron doping. The behavior of Calderón *et al.*'s model can be explained by

the unrealistically high ellipticity of the electron pockets. Calderón *et al.*⁴⁶ started from an eight-orbital model with nearest-neighbor Fe-Fe and Fe-As hopping and then removed the As orbitals within perturbation theory. By using the Slater-Koster approach, they were able to write the eighteen hopping integrals as functions of only four overlap integrals and the Fe-As bond angle; in the other models, these eighteen hopping integrals are free parameters, which gives much greater freedom in fitting the band structure. One can speculate that the smaller parameter space available to Calderón *et al.* is responsible for the unphysical doping dependence in their model. Among the remaining models, the monotonous increase of T_c for the model of Graser *et al.*, see Figs. 3 and 8(a), also contradicts available experimental data.^{17–21,23,24} The comparably high $(3z^2 - r^2)$ -derived flat band at the M point is responsible for this strong tendency to AFM order.³⁴ In contrast, the models of Kuroki *et al.* and Ikeda *et al.* show a dome of $(\pi, 0)$ order centered at moderate hole doping $\delta \approx -0.1$; for realistic maximum critical temperature $T_c \approx 165$ K there is no ordering at zero nominal doping, $\delta = 0$. Similar behavior is seen in the model of Graser *et al.* for sufficiently small interaction strength. In the first three models there are hence strong $(\pi, 0)$ spin fluctuations at weak doping, consistent with previous studies^{39,42,43} and the asymmetric doping dependence of the SDW phase observed in some experiments.^{5,17–24}

Our results again demonstrate the sensitive dependence of the magnetic order on small details of the band structure in the weak-coupling limit.³⁴ This is illustrated by the major discrepancies between the model of Graser *et al.* and the more realistic models of Kuroki *et al.* and Ikeda *et al.*, despite the very similar band structures of these three models. It is significant that the models of Kuroki *et al.* and Ikeda *et al.* were obtained by fitting to *ab initio* results for the experimental crystal structure of the FeAs planes, whereas the model of Graser *et al.* is based upon *ab initio* calculations for a relaxed structure. These two structures have rather different Fe-As bond angles, which has been identified as a crucial control parameter for pnictide physics.^{39,42,46}

In addition to the major role of the band structure, important details of the antiferromagnetic order were found to be controlled by the interaction strengths involving the xy orbital relative to the other orbitals. Under the common assumption of orbitally rotation-invariant interactions, the models of Kuroki *et al.*⁴² and Ikeda *et al.*³⁹ display $(\pi, 0)$ order at optimal doping (maximum SDW critical temperature T_c). Upon reducing the interactions involving the xy orbital, the optimal doping slightly shifts and the ordering vector tends to become weakly incommensurate: At the lowest reduction factor $V_{xy} = 0.7$, the AFM dome for the model of Kuroki *et al.* becomes entirely incommensurate, while for the model of Ikeda *et al.* there is a continuous change from incommensurate to commensurate order as one moves from stronger to weaker doping. Reducing V_{xy} in the model of Graser *et al.*,⁴³ we find that the dome with $(\pi, 0)$ order is almost

obscured by a second dome with weakly incommensurate order that has a smaller optimal doping.

We find that in all models commensurate $(\pi, 0)$ order is realized for an extended doping range. This shows that commensurate order can be stabilized in purely electronic models, but does of course not imply that mechanisms beyond the models considered here are unimportant in this respect. Indeed, the experimentally observed robustness of commensurate order suggests that some additional stabilizing mechanism is required, especially in the scenario of reduced V_{xy} . Accounting for the three-dimensionality of the Fermi surface may improve the nesting with a commensurate ordering vector. Most likely, though, the weak incommensuration we have found will result in commensurate order if magneto-elastic coupling is taken into account.

Our results allow us to distinguish the dominant nesting instability in the various models. The $(\pi, 0)$ order observed for orbitally rotation-invariant interactions originates mainly from the good nesting between the xy -derived parts of the Y pocket and the M pocket, as identified in Refs. 35–39. For reduced interactions involving the xy orbital, however, the nesting instability between the Γ and X pockets gives the highest ordering temperature, which corresponds to the scenario in Refs. 25–34. This mechanism is dominated by the yz orbital and produces a SDW with the ordering vector $\mathbf{Q} = (Q_x, 0)$, where $0.9\pi < Q_x \leq \pi$.

Our results therefore confirm the two proposals in the literature for a nesting instability in the pnictides, with their relative importance tuned by the parameter V_{xy} . This implies a crucial role for the As $4p$ orbitals, as their hybridization with the Fe $3d$ orbitals is ultimately responsible for the strong orbital dependence of the interaction potentials in an effective $3d$ theory.⁴⁷ It is therefore somewhat unsatisfying that the As orbitals do not enter the calculations more directly. Indeed, keeping the As $4p$ orbitals reduces the variation in the size of the Fe $3d$ Wannier functions, and hence the interaction strength is likely to show much less pronounced orbital dependence.^{47,51} A detailed comparison of the spin fluctuations in a realistic $3d$ - $4p$ model with those in a pure $3d$ model is therefore desirable.⁴⁹

V. SUMMARY

In this work we have presented an analysis of the instabilities responsible for magnetic order in the 1111 pnictides. Using the RPA we have determined the doping dependence of the SDW critical temperature and ordering vector in four different five-orbital models. For the three models proposed by Kuroki *et al.*,⁴² Graser *et al.*,⁴³ and Ikeda *et al.*,³⁹ we find that the observed $(\pi, 0)$ magnetic order is stabilized for hole doping, while in the model of Calderón *et al.*⁴⁶ an incommensurate SDW phase appears at electron doping, contradicting experimental results. We have studied the relative importance of the two

known nesting instabilities across the phase diagram of these models, and have identified the relative interaction strength in the xy orbital as a parameter that tunes the dominant mechanism leading to magnetic order. We have identified two models as giving particularly good agreement with experiment, and discussed the band structure features which lead to the poorer agreement for the others.

ACKNOWLEDGMENTS

The authors thank M. J. Calderón, M. Daghofer, T. Dellmann, P. Materne, J. Spehling, R. Valentí, M. Vojta, and B. Zocher for useful discussions. We acknowledge funding by the Deutsche Forschungsgemeinschaft through Priority Programme 1458.

-
- * jacob_alexander.schmiedt@tu-dresden.de
 † brydon@theory.phy.tu-dresden.de
 ‡ carsten.timm@tu-dresden.de
- ¹ Y. Kamihara, T. Watanabe, M. Hirano, and Hideo Hosono, *J. Am. Chem. Soc.* **130**, 3296 (2008).
 - ² M. Rotter, M. Tegel, and D. Johrendt, *Phys. Rev. Lett.* **101**, 107006 (2008).
 - ³ J. Zhao, Q. Huang, C. de la Cruz, S. Li, J. W. Lynn, Y. Chen, M. A. Green, G. F. Chen, G. Li, Z. Li, J. L. Luo, N. L. Wang, P. Dai, *Nature Materials* **7**, 953 (2008); J. Zhao, Q. Huang, C. de la Cruz, J. W. Lynn, M. D. Lumsden, Z. A. Ren, J. Yang, X. Shen, X. Dong, Z. Zhao, P. Dai, *Phys. Rev. B* **78**, 132504 (2008).
 - ⁴ Q. Huang, Y. Qiu, W. Bao, J. W. Lynn, M. A. Green, Y. Chen, T. Wu, G. Wu, and X. H. Chen, *Phys. Rev. Lett.* **101**, 257003 (2008); A. Jesche, N. Caroca-Canales, H. Rosner, H. Borrmann, A. Ormeci, D. Kasinathan, K. Kaneko, H. H. Klauss, H. Luetkens, R. Khasanov, A. Amato, A. Hoser, C. Krellner, and C. Geibel, *Phys. Rev. B* **78**, 180504(R) (2008).
 - ⁵ M. D. Lumsden and A. D. Christianson, *J. Phys.: Condens. Matter* **22**, 203203 (2010).
 - ⁶ S. E. Sebastian, J. Gillett, N. Harrison, P. H. C. Lau, C. H. Mielke, and G. G. Lonzarich, *J. Phys.: Condens. Matter* **20**, 422203 (2008); J. G. Analytis, R. D. McDonald, J.-H. Chu, S. C. Riggs, A. F. Bangura, C. Kucharczyk, M. Johannes, and I. R. Fisher, *Phys. Rev. B* **80**, 064507 (2009).
 - ⁷ M. Yi, D. H. Lu, J. G. Analytis, J.-H. Chu, S.-K. Mo, R.-H. He, M. Hashimoto, R. G. Moore, I. I. Mazin, D. J. Singh, Z. Hussain, I. R. Fisher, and Z.-X. Shen, *Phys. Rev. B* **80**, 174510 (2009).
 - ⁸ T. Shimojima, K. Ishizaka, Y. Ishida, N. Katayama, K. Ohgushi, T. Kiss, M. Okawa, T. Togashi, X.-Y. Wang, C.-T. Chen, S. Watanabe, R. Kadota, T. Oguchi, A. Chainani, and S. Shin, *Phys. Rev. Lett.* **104**, 057002 (2010).
 - ⁹ M. A. McGuire, A. D. Christianson, A. S. Sefat, B. C. Sales, M. D. Lumsden, R. Jin, E. A. Payzant, D. Mandrus, Y. Luan, V. Keppens, V. Varadarajan, J. W. Brill, R. P. Hermann, M. T. Sougrati, F. Grandjean, G. J. Long, *Phys. Rev. B* **78**, 094517 (2008); M. A. McGuire, R. P. Hermann, A. S. Sefat, B. C. Sales, R. Jin, D. Mandrus, F. Grandjean, and G. J. Long, *New J. Phys.* **11**, 025011 (2009).
 - ¹⁰ R. H. Liu, G. Wu, T. Wu, D. F. Fang, H. Chen, S. Y. Li, K. Liu, Y. L. Xie, X. F. Wang, R. L. Yang, L. Ding, C. He, D. L. Feng, and X. H. Chen, *Phys. Rev. Lett.* **101**, 087001 (2008).
 - ¹¹ J. K. Dong, L. Ding, H. Wang, X. F. Wang, T. Wu, G. Wu, X. H. Chen, and S. Y. Li, *New J. Phys.* **10**, 123031 (2008).
 - ¹² S.-L. Drechsler, H. Rosner, M. Grobosch, G. Behr, F. Roth, G. Fuchs, K. Koepf, R. Schuster, J. Malek, S. Elgazar, M. Rotter, D. Johrendt, H.-H. Klauss, B. Büchner, and M. Knupfer, arXiv:0904.0827.
 - ¹³ W. L. Yang, P. O. Velasco, J. D. Denlinger, A. P. Sorini, C.-C. Chen, B. Moritz, W.-S. Lee, F. Vernay, B. Delley, J.-H. Chu, J. G. Analytis, I. R. Fisher, Z. A. Ren, J. Yang, W. Lu, Z. X. Zhao, J. van den Brink, Z. Hussain, Z.-X. Shen, and T. P. Devereaux, *Phys. Rev. B* **80**, 014508 (2009).
 - ¹⁴ D. J. Singh and M.-H. Du, *Phys. Rev. Lett.* **100**, 237003 (2008).
 - ¹⁵ I. I. Mazin, D. J. Singh, M. D. Johannes, and M. H. Du, *Phys. Rev. Lett.* **101**, 057003 (2008).
 - ¹⁶ Y.-Z. Zhang, I. Opahle, H. O. Jeschke, and R. Valentí, *Phys. Rev. B* **81**, 094505 (2010).
 - ¹⁷ H.-H. Wen, G. Mu, L. Fang, H. Yang, and Z. Zhu, *Europhys. Lett.* **82**, 17009 (2008).
 - ¹⁸ G. Mu, L. Fang, H. Yang, X. Zhu, P. Cheng, and H.-H. Wen, *J. Phys. Soc. Jpn. Suppl.* **77**, 15 (2008).
 - ¹⁹ G. Mu, B. Zeng, X. Zhu, F. Han, P. Cheng, B. Shen, and H.-H. Wen, *Phys. Rev. B* **79**, 104501 (2009).
 - ²⁰ G. Mu, B. Zeng, P. Cheng, X. Zhu, F. Han, B. Shen, and H.-H. Wen, *Europhys. Lett.* **89**, 27002 (2010).
 - ²¹ C. Bernhard, A. J. Drew, L. Schulz, V. K. Malik, M. Rössle, C. Niedermayer, T. Wolf, G. D. Varma, G. Mu, H.-H. Wen, H. Liu, G. Wu, and X. H. Chen, *New J. Phys.* **11**, 055050 (2009).
 - ²² J.-H. Chu, J. G. Analytis, C. Kucharczyk, and I. R. Fisher, *Phys. Rev. B* **79**, 014506 (2009).
 - ²³ H. Chen, Y. Ren, Y. Qiu, Wei Bao, R. H. Liu, G. Wu, T. Wu, Y. L. Xie, X. F. Wang, Q. Huang, and X. H. Chen, *Europhys. Lett.* **85**, 17006 (2009).
 - ²⁴ M. Rotter, M. Tegel, I. Schellenberg, F. M. Schappacher, R. Pöttgen, J. Deisenhofer, A. Günther, F. Schrettle, A. Loidl, and D. Johrendt, *New J. Phys.* **11**, 025014 (2009).
 - ²⁵ V. Cvetkovic and Z. Tesanovic, *Europhys. Lett.* **85**, 37002 (2009); *Phys. Rev. B* **80**, 024512 (2009).
 - ²⁶ R. Yu, K. T. Trinh, A. Moreo, M. Daghofer, J. A. Riera, S. Haas, and E. Dagotto, *Phys. Rev. B* **79**, 104510 (2009).
 - ²⁷ P. M. R. Brydon and C. Timm, *Phys. Rev. B* **79**, 180504(R) (2009); *Phys. Rev. B* **80**, 174401 (2009).
 - ²⁸ J. Knolle, I. Eremin, A. V. Chubukov, and R. Moessner, *Phys. Rev. B* **81**, 140506(R) (2010).
 - ²⁹ J. Knolle, I. Eremin, A. Akbari, and R. Moessner, *Phys. Rev. Lett.* **104**, 257001 (2010); A. Akbari, J. Knolle, I. Eremin, and R. Moessner, *Phys. Rev. B* **82**, 224506 (2010).
 - ³⁰ M. Daghofer, A. Nicholson, A. Moreo, and E. Dagotto, *Phys. Rev. B* **81**, 014511 (2010).
 - ³¹ I. Eremin and A. V. Chubukov, *Phys. Rev. B* **81**, 024511 (2010).

- ³² A. B. Vorontsov, M. G. Vavilov, and A. V. Chubukov, *Phys. Rev. B* **81**, 174538 (2010).
- ³³ R. M. Fernandes and J. Schmalian, *Phys. Rev. B* **82**, 014521 (2010).
- ³⁴ P. M. R. Brydon, M. Daghofer, and C. Timm, *J. Phys.: Condens. Matter* **23**, 246001 (2011).
- ³⁵ H. Ikeda, *J. Phys. Soc. Japan* **77**, 123707 (2008).
- ³⁶ K. Kuroki, H. Usui, S. Onari, R. Arita, and H. Aoki, *Phys. Rev. B* **79**, 224511 (2009).
- ³⁷ H. Ikeda, R. Arita, and J. Kuneš, *Phys. Rev. B* **82**, 024508 (2010).
- ³⁸ R. Arita and H. Ikeda, *J. Phys. Soc. Japan* **78**, 113707 (2009).
- ³⁹ H. Ikeda, R. Arita, and J. Kuneš, *Phys. Rev. B* **81**, 054502 (2010).
- ⁴⁰ J. Knolle, I. Eremin, and R. Moessner, *Phys. Rev. B* **83**, 224503 (2011).
- ⁴¹ P. M. R. Brydon, J. Schmiedt, and C. Timm, *Phys. Rev. B* **84**, 214510 (2011).
- ⁴² K. Kuroki, X. Onari, R. Arita, H. Usui, Y. Tanaka, H. Kontani, and H. Aoki, *Phys. Rev. Lett.* **101**, 087004 (2008).
- ⁴³ S. Graser, T. A. Maier, P. J. Hirschfeld, and D. J. Scalapino, *New J. Phys.* **11**, 025016 (2009).
- ⁴⁴ Q. Luo, G. Martins, D.-X. Yao, M. Daghofer, R. Yu, A. Moreo, and E. Dagotto, *Phys. Rev. B* **82**, 104508 (2011).
- ⁴⁵ S. Raghu, Z.-L. Qi, C.-X. Liu, D. J. Scalapino, and S.-C. Zhang, *Phys. Rev. B* **77**, 220503(R) (2008).
- ⁴⁶ M. J. Calderón, B. Valenzuela, and E. Bascones, *Phys. Rev. B* **80**, 094531, (2009).
- ⁴⁷ T. Miyake, K. Nakamura, R. Arita, and M. Imada, *J. Phys. Soc. Jpn.* **79**, 044705 (2010).
- ⁴⁸ Y. Yanagi, Y. Yamakawa, and Y. Ono, *J. Phys. Soc. Jpn.* **77**, 123701 (2008).
- ⁴⁹ T. Schickling, F. Gebhard, J. Bünemann, L. Boeri, O. K. Andersen, and W. Weber, *Phys. Rev. Lett.* **108**, 036406 (2012).
- ⁵⁰ L. Boeri, O. V. Dolgov, and A. A. Golubov, *Phys. Rev. Lett.* **101**, 026403 (2008).
- ⁵¹ V. Vildosola, L. Pourovskii, R. Arita, S. Biermann, and A. Georges, *Phys. Rev. B* **78**, 064518 (2008).
- ⁵² E. Kaneshita, T. Morinari, and T. Tohyama, *Phys. Rev. Lett.* **103**, 247202 (2009).
- ⁵³ E. Bascones, M. J. Calderón, and B. Valenzuela, *Phys. Rev. Lett.* **104**, 227201 (2010).
- ⁵⁴ A. M. Oleś, *Phys. Rev. B* **28**, 327 (1983).
- ⁵⁵ E. Dagotto, T. Hotta, and A. Moreo, *Phys. Rep.* **344**, 1 (2001).
- ⁵⁶ G. Xu, W. Ming, Y. Yao, X. Dai, S.-C. Zhang, and Z. Fang, *Europhys. Lett.* **82**, 67002 (2008).